HAL open science

Brightness variations of the northern 630nm intertropical arc and the midnight pressure bulge over Eritrea

R. H. Wiens, S. Habtemichael, F. Andemariam, K. Welday, J. Criswick, S. Brown, S. Sargoytchev

To cite this version:

R. H. Wiens, S. Habtemichael, F. Andemariam, K. Welday, J. Criswick, et al.. Brightness variations of the northern 630nm intertropical arc and the midnight pressure bulge over Eritrea. Annales Geophysicae, 2004, 22 (9), pp.3251-3259. hal-00317649

HAL Id: hal-00317649

https://hal.science/hal-00317649v1

Submitted on 18 Jun 2008

HAL is a multi-disciplinary open access archive for the deposit and dissemination of scientific research documents, whether they are published or not. The documents may come from teaching and research institutions in France or abroad, or from public or private research centers.

L'archive ouverte pluridisciplinaire **HAL**, est destinée au dépôt et à la diffusion de documents scientifiques de niveau recherche, publiés ou non, émanant des établissements d'enseignement et de recherche français ou étrangers, des laboratoires publics ou privés.

Annales Geophysicae (2004) 22: 3251–3259
SRef-ID: 1432-0576/ag/2004-22-3251
© European Geosciences Union 2004

Annales Geophysicae

Brightness variations of the northern 630 nm intertropical arc and the midnight pressure bulge over Eritrea

R. H. Wiens[1,*], S. Habtemichael[1], F. Andemariam[1], K. Welday[1], J. Criswick[2], S. Brown[2], and S. Sargoytchev[2]

[1]Department of Physics, University of Asmara, P.O. Box 1220, Asmara, Eritrea
[2]CRESS, York University, 4700 Keele St., Toronto, M3J 1P3, Canada
[*]now: 123 Ninth Street, Toronto, M8V 3E5, Canada

Received: 2 September 2003 – Revised: 21 May 2004 – Accepted: 9 June 2004 – Published: 23 September 2004

Part of Special Issue "Equatorial and low latitude aeronomy"

Abstract. The nightglow brightness at 630 nm from the thermospheric O(^{1}D) layer was monitored nightly at Asmara, Eritrea (15.4° N, 39.9° E, 7° N dip) with an all-sky imager. Averages of north-south strips of the images enabled contour plots of brightness on a latitude vs. local time grid. The contours show the movement of the intertropical arc southward before midnight, staying just north of Asmara after midnight, and gradually brightening to a maximum at 02:00 h local civil time, 02:00 LT, after which it disappears before dawn. It is argued that all features of the plots can be explained by known mechanisms capable of driving ions along magnetic field lines, including the fountain effect, summer to winter transequatorial winds, and the midnight pressure bulge.

The 02:00 LT brightness maximum is the most striking and the most persistent feature in the data. The persistence of the location of the 02:00 LT brightening is attributed to a pressure bulge centered on the geographic equator at midnight and extending to higher latitudes with increasing local time in both the winter and the summer hemispheres. The bulge is shown to be stronger near solstice than near equinox, confirming earlier work.

Key words. Atmospheric composition and structure (airglow and aurora) – Ionosphere (equatorial ionosphere) – Meteorology and atmospheric dynamics (thermospheric dynamics)

1 Introduction

The behavior of almost any measurable quantity in the tropical ionosphere is complicated because it is always subject to a variety of dynamical processes as well as the basic photochemical ones. Most studies of the complex dynamics have taken place in the American longitudinal sector, largely because of the major radar installations at Arecibo and Jicamarca. The ability of these incoherent scatter radars to measure many important quantities naturally attracts other instruments to participate in multi-station, multi-instrument campaigns and in related permanent installations, which adds to the richness of our understanding of the dynamical processes. However, the American sector has an unusual relation between its geographic coordinates, which order the neutral atmosphere, and its magnetic coordinates, which control the motions of charged particles. More global in approach, but less specific regionally, are satellite measurements, but data from these are usually averaged indiscriminately over all longitudes. There, is therefore, a role for ground-based measurements at other longitudes to challenge and extend the generality of results that seem to work well in the regional or the space-based context. Reports from India have for a long time performed such a role, but tropical Africa has traditionally contributed data from short-lived stations that appear in the literature as basically episodic. Because of their scarcity, quality African data should be employed to test dynamical principles for applicability in this longitude sector whenever they become available. An excellent opportunity to do so was provided by our all-sky imager operating in Asmara , Eritrea, at 15.4° N, 39.9° E, 7° N dip. The location is ideal for observations of the 630 nm O(^{1}D) nightglow, because the northern member of the intertropical arcs, two bands of enhanced red line nightglow that encircle the Earth paralleling the magnetic equator at nominal dip latitudes of ±15°, is usually apparent in the northern sky using appropriate equipment, and the magnetic declination is less than 2°, meaning that magnetic field lines are oriented in the geographical northward direction. Our Asmara data are not the first red line (630 nm) nightglow measurements to be reported from Africa. Indeed, the intertropical arc was discovered by Barbier et al. (1961) at Tamanrasset in southern Algeria, and we shall have occasion to refer to work by Weill et al. (1968) in Ethiopia and Skinner et al. (1977) in Kenya. All of these writers report on several nights of data. Our advance on their work lies in our having a high resolution instrument observing on enough nights to provide meaningful average monthly behavior from which we can discern details only hinted at previously.

Correspondence to: R. H. Wiens
(rwiensc521@rogers.com)

The $O(^1D)$ nightglow red line arises from the neutralization of the dominant F-region ion, O^+, in two steps. The first is a charge exchange with O_2:

$$O^+ + O_2 \rightarrow O_2^+ + O\,. \tag{1}$$

The molecular ion is then readily destroyed by an ambient electron in the dissociative recombination reaction

$$O_2^+ + e \rightarrow O(^1D) + O(^3P)\,. \tag{2}$$

Although other combinations of excited O atoms are possible in reaction (2), (^1D) is always part of the scheme, and it is this state which after about 110 s decays to the (^3P) ground state with the emission of a photon of wavelength 630.0 or 636.4 nm. Increasing the density of the O_2 increases the probability of these reactions taking place, so that when ionization consisting of O^+ ions and free electrons is driven to a lower altitude where O_2 density is greater, the emission rate of the red line increases. Although the emission takes place over a broad range of altitudes, the maximum rate in the nightglow occurs around 280 km, and we will use that altitude as the nominal one where the reactions are most likely.

The intertropical arcs were identified by Barbier and Glaume (1962) as the optical expression of the equatorial ionization anomaly (EIA), which is driven by the fountain effect. Plasma lifted at the equator by an eastward directed electric field during the day diffuses down the magnetic field lines under the influence of gravity away from the equator until it reaches altitudes, around 280 km, where recombination by Eqs. (1) and (2) is likely. Around 21:00 LT the electric field at the equator reverses, and the ionization lowers. As shown by Anderson (1973) this reversal results in the anomaly moving equatorward and diminishing throughout the rest of the night. The global nature of the intertropical arc system following the magnetic dip equator was clearly demonstrated from OGO satellite data by Chandra et al. (1973). Thuillier et al. (2002) reviewed and demonstrated the role of transequatorial neutral winds in causing seasonal variations in arc brightness. When there is a transequatorial wind, collisions between neutrals and ions move the ions forward, but they are constrained to move along magnetic field lines which carry them upward or downward depending upon the local geometry. Above the dip equator the upwelling ions are thus driven along initially horizontal field lines by neutrals in the wind blowing from the summer hemisphere and then downward to enrich the intertropical arc on the winter side of the equator. The neutral winds, in turn, are driven by solar tides, so it is expected that brightness variations in the intertropical arc should bear the signature of tidally driven winds in the middle thermosphere, that is, in the F-region of the ionosphere. The diurnal tide drives air from the warm summer hemisphere across the geographic equator into the winter hemisphere toward the anti-solar point.

When the characteristics of the intertropical arcs were first being explored, Greenspan (1966) noticed that his ship-borne 630-nm photometer showed a persistent brightness maximum at midnight in the eastern Pacific sector at the latitude of the EIA. Such brightenings were later reported from Arecibo by Nelson and Cogger (1971) and given an interpretation in terms of the abatement of an equatorward wind by Behnke and Harper (1973). An equatorward wind at Arecibo would drive ionization upward along magnetic field lines from the EIA, and an abatement would allow the ionization in the EIA to reach lower altitudes and dissociatively recombine more quickly. Harper (1973) found that ion temperatures at Arecibo reached a maximum that coincided in local time with the equatorward wind abatement. He proposed tentatively a lateral V shaped pressure bulge with vertex at the equator and branches increasing in latitude with increasing local time in both hemispheres. A neutral temperature enhancement was seen around midnight in the tropics by mass spectrometer in situ measurements on the AE-E satellite by Spencer et al. (1979), who gave it the name midnight temperature maximum (MTM). An initial explanation in terms of tides was offered by Mayr et al. (1979), who showed that ion-neutral momentum coupling was able to propagate energy via neutral winds from the sub-solar temperature and ionization maximum, to form a smaller maximum in temperature and pressure at the opposite, anti-solar point, in effect generating a semidiurnal tidal component. Their mechanism supposes that neutral winds blowing away from the sub-solar temperature maximum are weakened on the dayside by ion drag; when they reach the nightside, ion drag is reduced and the neutral wind is increased. Convergence of these enhanced nightside winds causes downwelling and increased heating, and therefore creates a pressure and temperature bulge at the anti-solar point. Back pressure from this pressure bulge leads to an abatement of the equatorward wind in the vicinity of Arecibo. The downwelling, of course, moves the ionization down field lines to where the collision frequency is increased and the red line emission rate is increased. Herrero et al. (1983) demonstrated how an additional semidiurnal tidal component with strong seasonal dependence is generated by the heating of the ionosphere by solar EUV radiation. It is the interaction of these two semidiurnal tidal components which gives the MTM its geographical and seasonal signature. The MTM, according to Herrero and Spencer (1982), starts at the geographic equator at midnight and moves toward higher latitudes with increasing local time. The seasonal signature is a stronger branch in the summer hemisphere than in the winter hemisphere, with cancellation leading to a weak presence at equinox. These processes are clearly described in the excellent review by Herrero et al. (1993). Mayr et al. (1979), Hedin et al. (1980) and Herrero and Mayr (1986) showed the importance of terdiurnal as well as semidiurnal tidal components in describing upper thermosphere dynamics, in general, and MTM effects, in particular. Fesen (1996) showed that, in addition to the ion-neutral momentum coupling and solar EUV heating mechanisms, enhanced propagating semidiurnal tides of modes (2,2) and (2,3) from the lower atmosphere were needed to simulate the MTM in the NCAR general circulation model, the TIEGCM (thermosphere ionosphere electrodynamic general circulation model). However, Colerico and Mendillo (2002) point out that the TIEGCM at

its best fails to predict observed MTM amplitudes and the poleward motion of the maximum. They suggest that more detail is required, including terdiurnal tidal components from the lower atmosphere.

In what follows we present all-sky imager data of the red line nightglow over Eritrea arranged as brightness contours on a latitude vs. local time grid for the months of September 2001 to May 2002, a period during which the solar activity and hence the EUV heating rate was at the cycle maximum. Our data verify and extend previous reports on the behavior of the intertropical arc in the African sector and add details that can be attributed to the presence of the midnight pressure bulge, or MPB. Qualitative descriptions are offered for how the fountain effect and the MPB can be used to explain all aspects of the red line behavior exhibited in our monthly contour plots.

2 Experimental details

2.1 Equipment

The instrument employed in this experiment is called YASAC for York All-Sky Airglow Camera, from York University. It was described in detail by Criswick (1996), who used it to show the dynamic nature of gravity wave activity expressed by $O(^1S)$ and $O_2(^1\Sigma)$ nightglow emissions. It now employs a Kodak KAF1300 1300×1028 pixel CCD, having 16×16 μm pixels and cooling to −30°C. Light is collected by a fisheye lens of 8-mm focal length, collimated by a 135-mm lens, passed through an interference filter, and imaged onto the CCD using a 50-mm lens. All of the lenses are Nikon 35-mm format compound photographic lenses. The interference filter is carried on a wheel of eight such filters driven by a stepping motor on command from a personal computer. The primary filter is centered at 630.6 nm to accept the $O(^1D)$ nightglow red line at 630.0 nm. Its width is 1.8 nm, the bandwidth and position chosen so as to minimize brightness variation (or optimize the "flat fielding") over the 0° to 5° incidence angles set by the lens geometry. The images are collected by a 256×256 array of superpixels, each comprising a 4×4 subarray of elementary pixels. Accumulated counts from the superpixels are stored in 16-bit FITS format for easy imaging using Smithsonian Astronomical Observatory software. The operating cycle included obtaining images through filters centered at 572.3 and 677.4 nm to monitor background light as well as the 630.6-nm red line filter. The exposure time for each filter was 60 s, so that a complete measurement was made in just over 3 min. The instrument was operated on the roof of the main University of Asmara building, repeating this three-filter cycle during all hours of darkness.

2.2 Data analysis

The routine used to extract the data begins with a removal of bright spots caused by cosmic ray impact. An equivalent dark image, a long-time average dark image normalized to match the count rate at the unexposed corners of each image, is then subtracted from the sky image. YASAC was oriented so that the north-south direction on an image corresponds to the horizontal axis of the CCD array. Thirty rows of pixels centered on the zenith are averaged to produce a linear array of count rates. The ends of the array are chosen to correspond to horizontal distances of 10 latitude degrees south and 10° north of the station, projected on the ground, assuming an emission altitude of 280 km. Such a strip is produced not only for the red image, but for the shorter and longer wavelength comparison images as well. A weighted mean of the two background filter arrays is subtracted, pixel by pixel, from the red image. The weighting factor is taken from an overcast sky measurement on the assumption that the only light seen under this condition is city background and that it is spectrally continuous. The remaining array is therefore free of both dark count and city light contamination. It is then corrected for flat field and van Rhijn effects, and mapped from pixel divisions (linear function of zenith angle) to half-degree latitude spacings. At 10° elevation angle, the 280-km projection is about 10 latitude degrees from the camera location. Bin count rates averaged over each half degree are thus linear arrays extracted from each red image. The civil time of each red image is stored with this array.

With each red nightglow image thus represented by a linear array of brightness as a function of latitude, it is necessary only to place the linear arrays side by side in a keogram fashion to develop a rectangular array of latitude vs. local time with each intersection point represented by the appropriate average integrated count rate. The arrays are, in fact, averaged further into half-hour bins for one month at a time. A MATLAB contouring algorithm then produces the latitude-local time plots of the red line relative emission rate described in Sect. 3.

2.3 Uncertainties

The standard deviation of the accumulated count on a superpixel from a typical north-south strip in a red line image is approximately 5 or 6 counts. When averaged over the half-degree latitude bins, this noise level becomes quite small and is neglected here. A more serious concern is in the background subtraction procedure. The subtraction process used here is dependent upon the spectral distribution of the background light. This is not as constant as one would hope, particularly since moon and star light are very different spectrally from city light, and the varied combinations change quickly in time and direction. In particular, a wisp of cloud can produce either an anomalously high or an anomalously low count rate. Therefore, each image was visually inspected for any hint of cloud or dome condensation and rejected if it was not problem-free. Condensation problems are most prevalent in the early evening, causing us to discard all readings before 21:00 LT. Nevertheless, we estimate that in any subtraction the uncertainty of the difference between the airglow component and the background could be as large as ±50 counts. These differences when combined into latitude

Table 1. Data summary.

Month	F10.7 (W/m^2 Hz)	Ap	No. of Nights
Sep. 2001	191.3	12.8	12
Oct. 2001	191.9	12.0	10
Nov. 2001	193.7	12.0	18
Dec. 2001	193.9	12.2	17
Jan. 2002	194.6	12.3	13
Feb. 2002	197.2	12.8	18
Mar. 2002	195.7	12.9	21
Apr. 2002	191.5	13.2	17
May. 2002	188.0	13.3	10

bins are typically averages of 4; about 36 latitude bins appear in an average of one month of half-hour time segments. Formally, this results in a final uncertainty of only 3 counts, but we suggest a conservative ±10 counts to cover most latitudes, and ±3 for those nearest the station. These uncertainties are quite small compared to the 100-count contour intervals that we present.

YASAC data used here are uncalibrated, justified by our emphasis on the dynamical features of the variation rather than the photochemical. Noting that the intertropical arc over Eritrea has never been reported as a visual event, we would say the maximum brightness is always less than one kilorayleigh, but likely on the order of half that amount.

2.4 Data summary

We show monthly averages of relative (uncalibrated) 630.0-nm brightness. It is useful to note that the data represent the solar activity maximum according to the NOAA Space Environment Center smoothed monthly averages of the 10.7-cm radio flux listed in Table 1. For the most part this period was not marked by great geomagnetic activity, as shown by the mean monthly Ap indices which lie between 12.0 and 13.3, but storms in April and May could seriously affect the averages. Also listed in the table is the number of nights in the month from which data were useable, excluding conditions of cloud, excessive moonlight, and instrumental problems.

3 Results

3.1 Presentation details

The results of the brightness averaging are displayed as color contours on latitude vs. local time grids in Fig. 1, one for each month of data described in Table 1. Data are presented for only nine months, excluding June, July, and August because of the major rainy season in Asmara at that time. The latitude axis is offset to make the overhead position at Asmara, 15.4° N, read 0, marked on each frame by a horizontal line. The latitude axis thus extends from 5° N to 25° N geographic, or, with Asmara at 7° N dip, it extends from 3° S to

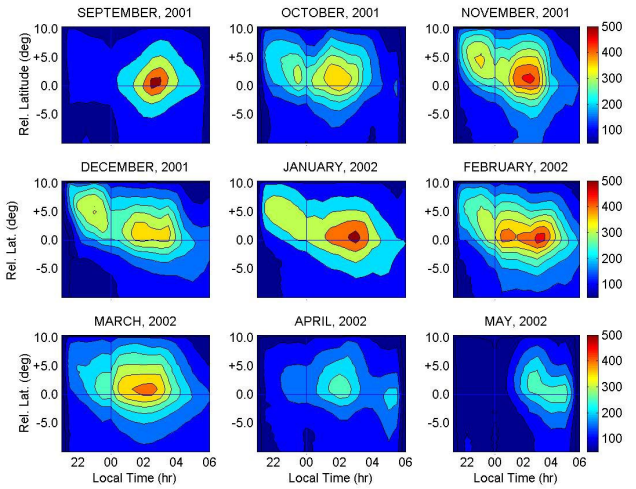

Fig. 1. Latitude-local time contour plots of O[^{1}D] 630-nm brightness over Asmara. Vertical axes place Asmara (15.4° N geographic or 7° N dip) at 0° latitude, marked by horizontal line. Vertical line marks local midnight, 00:00 LT.

17° N in magnetic dip latitude. The local time axis employs East Africa civil time (LT), which precedes UTC (Universal Coordinated Time, formerly UT) by three hours. Asmara's longitude gives a local mean time of 2.6 h before UTC, so that local mean midnight falls in the half-hour preceding the vertical line at the civil 00:00 LT position. The color axis is shown on the right side of the page. Contours are drawn for every 100 counts using the same scale for every frame to facilitate comparison between different months.

3.2 Latitude, local time brightness distribution

The basic nocturnal variation of the 630-nm (OI) brightness is best appreciated by looking at the center row of images in Fig. 1 for the three winter months, December, January, and February. The outer contours, indicating 200 counts, show a band of brightness extending from near the north horizon at the top of the image, to approximately overhead at the start of the night. This band of brightness moves southward fairly rapidly until well after midnight, then remains stationary or moves southward only slowly until it is lost around 04:00 LT, well before dawn. This band of brightness is the intertropical arc, generally regarded as the optical manifestation of the EIA, known to result from the fountain effect.

We notice two brightness maxima imbedded in the intertropical arc contours. The pre-midnight maximum is particularly evident in November and December at 23:00 LT, 5° north of Asmara, or 12° N dip. We identify this pre-midnight brightness enhancement as the result of an enhanced fountain effect associated with the pre-reversal electric field enhancement. In all frames there is a brightness minimum at midnight, which is clearly evident as a pinching of the 300-count contours for October through March. A more pronounced maximum appears in the post-midnight period, when the arc has reached its minimum latitude. We argue that this very

persistent post-midnight enhancement is the regional effect of the midnight pressure bulge, MPB, a facet of the midnight temperature maximum, or MTM. After this maximum, the red line brightness decreases until the arc is no longer distinguishable from the diffuse nightglow background. The intertropical arc terminates well before dawn.

3.3 Seasonal variation

The seasonal dependence of the red nightglow brightness is seen by comparing all the monthly images of Fig. 1. Although the intertropical arc (as marked by the 200-count contours) is well developed from October through February, its horizontal (local time) extent is greatly curtailed in September, March, and April, and non-existent in May, when all that remains is the post-midnight maximum. Thuillier et al. (2002) emphasized that the fountain effect that produces the intertropical arcs of essentially equal brightness in the Northern and Southern Hemispheres, is modulated by transequatorial winds directed from the warm summer hemisphere into the cool winter hemisphere. Thus, May represents summer conditions in Asmara in which the winds are primarily equatorward, while September, March, and April show the weak arc of equinox conditions when the meridional wind blows weakly with almost equal probability in either direction. The remaining months, October through February, are then winter months in the sense of poleward wind and a fully developed arc. The pre-midnight maximum also appears to comply with this description.

The post-midnight maximum undergoes brightness variations from month to month, but it appears in all months studied and, most strikingly, it appears at essentially the same location in every month. The location of the brightest point in the gridded monthly data is listed in Table 2, where it is seen that the magnetic latitude is (8° N+1°) dip, and the local time is (2.0±0.5) h LT. We notice from Table 2 that the post-midnight or, more precisely, the 02:00 LT maximum, is brightest in both September and January. In fact, the January brightness is the culmination of a winter buildup and is followed by a decay as equinox is approached. December seems weak, but it is listed twice to show that the peak is spread over two latitude bins, which reduces the apparent peak value. April and May brightnesses are interpreted with caution because major geomagnetic storms occurred during the periods when most of the data were gathered. Storm effects will be the subject of a later paper and are not treated here. It is also noticed that some light from the dawn enters these plots as a contaminant near 06:00 LT. Nevertheless, the maximum is well defined in these two months, albeit at its weakest. We can imagine that the 02:00 LT maximum builds gradually through the summer months to its greatest brightness in August or September, making the solstice values large and the equinox values small. The abrupt decrease in brightness from September to October suggests that an equinox minimum condition follows the actual equinox date perhaps by several weeks.

Table 2. Post-midnight maximum characteristics.

Month	Dip Latitude (° N)	Local Time (h)	630 nm Brightness
September 2001	9.5	2.0	525
October 2001	10.0	1.5	400
November 2001	10.5	2.0	463
December 2001	10.0	1.5	379
December 2001	10.5	1.5	379
January 2002	9.5	2.5	526
February 2002	9.0	2.5	465
March 2002	10.0	2.0	417
April 2002	10.0	1.5	282
May 2002	10.5	2.5	268

3.4 Meridional wind inference

Over Asmara, 7° north of the magnetic dip equator, magnetic field lines point downward toward the north. Any poleward neutral wind by ion-neutral collisions forces ions down the field lines deeper into the atmosphere where the likelihood of recombination is increased and therefore the red line nightglow brightness is enhanced. An equatorward wind has the opposite effect. In this sense, then, the plots for October through April, which show, on average, fully developed cases of the intertropical arc (following the 200-count contours), indicate poleward winds, and since most of these months are the winter months, this is a simple confirmation of the neutral winds blowing from the warmer summer hemisphere into the cooler winter hemisphere, as discussed by Thuillier et al. (2002). The equinoctial months of March and April show weak arc development, indicating in this picture weak transequatorial winds or equal likelihood of such winds being northward or southward. May shows no arc development and September very little, just local brightening around the 02:00 LT maximum. We would say that this is the basic summer condition to the extent that we are able to observe it, with neutral winds blowing from the summer hemisphere across the equator into the winter hemisphere, giving equatorward winds over Asmara and no intertropical arc.

The pre-midnight maximum that is evident in the October through February plots is simply the result of an enhanced fountain effect associated with the pre-reversal electric field enhancement, as discussed below, subject to the same seasonal wind modulation.

After midnight the EIA weakens and moves south according to Anderson (1973). In Fig. 1 it is seen as having been overcome or even replaced by the post-midnight brightness enhancement. This post-midnight brightening at 02:00 LT can be interpreted as a wind perturbation that pushes neutral air poleward and drives ions downward with resultant red line brightening. Such a wind can be attributed to the MPB, as we discuss in the next section. Our data show that its location is quite constant in all months studied, but that it varies in strength seasonally as described in the previous subsection,

that is, weak near the equinoxes and strongest shortly after the solstices.

4 Discussion

4.1 Intertropical arc morphology

The morphology of the intertropical arc presented here is in close agreement with the description given by Weill et al. (1968). Observing from Debre Zeit, Ethiopia, at 8.8° N, 39.0° E or −0.7° dip in December and January of 1966/1967 with a meridian and azimuth scanning photometer, they saw the arc move south before midnight, come to rest and brighten after midnight, and then, after reaching a maximum around 03:00 LT, fade away. Our data corroborate their findings, but add a great deal of detail. In particular, because of their location 7° south of Asmara, they would not have been able to reliably measure the north side of the arc. The north side of the arc was, on the other hand, measured from Granada, Spain, by Battaner and Pardo (1972). Their red line brightening starts near their southern horizon at about 20:50 LT and disappears over that horizon by 23:00 LT, in good qualitative agreement with what is shown here. Spaceborne experiments, like OGO 4 and 6 (Chandra et al., 1973; Thuillier et al., 1976), described the global extent of the arcs, but did not do local time studies. Thus, what we report here about the location and behavior is consistent with, confirms, and adds detail to what may be regarded as the well-known phenomenon of the intertropical arc.

The behavior of the EIA generated by the fountain effect is graphically presented by Hanson and Moffett (1966) and by Anderson (1973). The eastward electric field drives ionization upward at the dip equator during the day and early evening. Under the influence of gravity and meridional winds, ions diffuse down the field lines to higher latitudes, forming the crest of the anomaly at about 15° dip. The electric field reverses at about 21:00 LT, causing a downward ion drift at the equator and lowering the equatorial F-layer there. The reversed fountain during the rest of the night causes the crests to weaken and move equatorward by diffusion. The result for Asmara is that the EIA moves south before midnight and remains there or moves slowly southward the rest of the night, diminishing in ion concentration.

The pre-midnight brightening that we see so prominently in the winter months is due to the enhanced fountain effect described by Whalen (1998). He studied the EIA using IGY data from a chain of South American stations to show that the following sequence occurs. In the early evening the F-region dynamo provides the eastward field that lifts the ionization that gives the fountain effect. When the Sun sets on the E-layer, the conductivity at E-layer heights disappears, and the eastward E-field increases which increases the fountain effect. The red line brightness enhancement we see in this picture coincides with the occurrence of the pre-reversal enhancement of the equatorial electric field. Whalen's (1998) study compared two nights which showed that the larger the equatorial vertical drift velocity, the greater the ionization at the EIA, and we may add the greater the red line brightness at the intertropical arc. The magnitude of this enhancement in our data shows a strong seasonal variation which we attribute to modulation by the transequatorial wind.

4.2 Midnight pressure bulge

What is seen as the post-midnight brightness enhancement of the 630-nm nightglow in our data is similar to the midnight maximum first reported by Greenspan (1966) in the American sector, now regarded as the first indication of the midnight temperature maximum, MTM, and by Nelson and Cogger (1971) at Arecibo. Weill et al. (1968) reported the same type of brightening in the east Africa sector but occurring at 03:00 LT rather than midnight. Again in the American sector, Sobral et al. (1978) found regular brightenings of the red line shortly after midnight in the vicinity of Arecibo (29° N geomagnetic) which coincided with an equatorward wind abatement and a descent of the F-layer. The brightenings propagated northward at speeds of about 300 m/s. Herrero and Meriwether (1980) studied such brightenings as meridional intensity gradients (MIGs) and attributed them to a midnight pressure bulge located at the anti-solar point, meaning north of the equator during the northern winter. Much of our current understanding of the MTM derives from the Atmospheric Explorer E satellite (AE-E). Volume emission rates at 630 nm were studied by Abreu et al. (1982) using AE-E data from November 1980 to January 1981. Binning all global data from the equator to 10° N (geographic) they found a maximum brightness at a local time of 02:50 LT and an altitude of 260 km, with a lesser one at 22:00 LT and 290 km, just as we report here. With data from the NATE (Neutral Atmosphere and Temperature Experiment) instrument on the same satellite, Herrero and Spencer (1982) organized neutral temperature data from 1977 and 1978 into contour plots on a latitude vs. local time grid for different seasons and concluded that in winter a temperature ridge crossed the equator at midnight, reached 10° N by 04:00 LT, and 15° S at 21:00 LT. The summer plot of Herrero and Spencer (1982) suggests a lateral V shaped ridge, as does a latitude-local time plot of meridional wind reversals of Herrero et al. (1993), in which the latitude of maximum pressure increases with increasing local time in both hemispheres. NATE neutral wind data studied from the same period by Goembel and Herrero (1995) confirmed that the pressure bulge follows similar behavior as the temperature maximum.

With this background, we propose that the lateral V MPB, first suggested by Harper (1973) and depicted in Fig. 2, represents the best model to explain the 02:00 LT brightening that is such a striking and persistent feature in the monthly average red line brightness plots of Fig. 1. The MPB is above the geographic equator at midnight and extends to higher latitudes in both the winter and the summer hemispheres with increasing local time. At 02:00 LT the north arm reaches a latitude at which the poleward wind component that it generates pushes ions forward and down the field lines to cause

a red line brightness enhancement. This occurs when the MPB crosses a field line that intersects with the atmosphere at about 280 km at 16° N (geographic) in our case. According to the San Marco 3 and 5 satellite measurements of Arduini et al. (1997), the midnight density bulge has its maximum at an altitude of about 350 km or less. The field line that intersects with the 280-km level at 8° N dip crosses the dip equator at an altitude of 411 km (using the well-known relationship for a dipole field that $r=R_0\sin^2\theta$, where θ is colatitude, and R_0 and r are the geocentric distances to the field line apex and any field line point, respectively) and the 350-km level at 14.5° N. Therefore, in Fig. 2 the MPB is shown crossing the 14.5° N latitude at 02:00 LT, in order to brighten the red line emission at 16° N at that time. The effect of the MPB is not seen in our data until it passes the dip equator, which, according to Fig. 2, does not happen until about 01:00 LT. The reason is that after midnight the ion drift is downward at the dip equator, making it an effective barrier to horizontal ion transport. As the MPB passes north of the anomaly region, ions are less abundant and the bulge provides an equatorward wind to the Asmara region, effectively quenching the arc by 04:00 LT. Since the same red line brightening occurs in the same place in both summer and winter, we suppose that the lateral V is symmetrical about the geographic equator, as shown in Fig. 2. The same structure applies to the equinox periods, although the pressure of the MPB is reduced at these times.

Skinner et al. (1977) observed the southern intertropical arc region in the east Africa sector with a red line photometer from Olorgesaile (1.6° S, 36.4° E). They reported an equatorward (northward) moving arc before midnight similar to what we observed, but after midnight, the red line brightness diminished rapidly and did not recover. According to our lateral V model, shortly after midnight the MPB is south of their station causing equatorward winds, and with the station being well south of the dip equator, these winds lift ionization and reduce the nightglow brightness. The lateral V of Fig. 2 thus seems consistent with what we know of east African red nightglow behavior.

The red line brightness patterns observed at any station will depend on the geometric relationship between geographic and magnetic coordinate systems in that region. Most ground-based studies pertaining to the midnight pressure bulge or the MTM have been conducted in the American sector, and much of that at Arecibo which magnetically is a mid-latitude station. The differences between America and Africa were evident in the earliest reports, with Greenspan (1966) reporting the maximum brightness at midnight near Peru and Weill et al. (1968) seeing it in Ethiopia at 03:00 LT. Thus, Colerico et al. (1996) plot the passage of a brightness wave that they associate with the MTM. We do not see evidence for that brightness wave signature in our averaged data, but we note that if we suppose the pressure bulge to start at the geographic equator at 00:00 LT and to intersect with latitude 14.5° N at 02:00 LT, as in Fig. 2, then the azimuth of its direction is, on average, 64° E of N and its speed is 514 m/s. Colerico et al. (1996) claim for their midnight

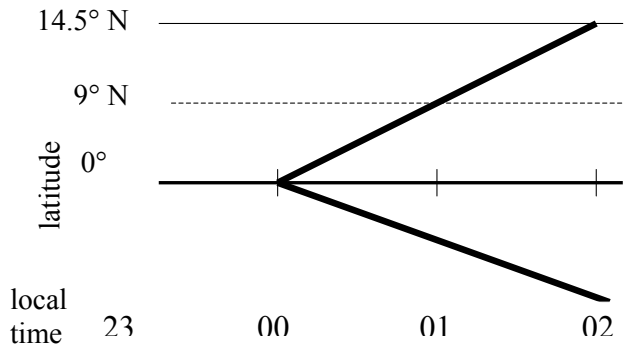

Fig. 2. Lateral V structure of the midnight pressure bulge adopted here. Dark lines represent ridge of high pressure shown crossing the dip equator at 9° N and the 14.5° N latitude, from which ions are driven downward to the maximum at 16° N. Southern arm is mirror image of northern arm.

brightness wave in October 1994 a speed of 356 m/s, with an orientation of 45° E of S in the Southern Hemisphere, with angles varying from 12° to 67°. The speeds reported by Sobral et al. (1978) from Arecibo as lying between 290 and 340 m/s agree with those of Colerico et al. (1996), both being considerably smaller than our African estimate. At Cachoeira Paulista (23° S, 45° W, 30° S dip) in Brazil, F-region winds were found by Batista et al. (1997) to have a strong poleward component at 02:00 LT during the winter solstice period and a strong equatorward component at 04:00 LT in both the winter and summer solstice periods. These features, which they attribute to the passage of the MPB, agree well with what we have reported here. The Indian sector has a geographic-magnetic geometry similar to that of Africa, and we might expect to see the same MPB characteristics there as here. Ranganath Rao and Sastri (1994) measured temperatures with a red line Fabry Perot interferometer at Kavalur (12.5° N, 78.5° E, 9.5° N dip) and found it reached a maximum as late as 02:00 LT in February 1992, but occurred progressively earlier as equinox approached. The only evidence we have to show such a seasonal change is the rather wide spread in local time of our February post-midnight maximum. Sastri et al. (1994) show northward winds peaking at 02:00 LT with equatorward surges at 00:00 LT and 05:00 LT in December 1992, at Sriharikota (13.7° N) that agree well with the brightening and the wanings we see at these times. Likewise, Hari and Krishna Murthy (1995) show the same poleward wind at 02:00 LT in their averaged winter data, and an equatorward wind after that.

4.3 Model comparisons

The NCAR Thermosphere Ionosphere Electrodynamic General Circulation Model, TIEGCM, was employed by Thuillier et al. (2002) to simulate three nights of WINDII data in which the meridional winds associated with the formation of the intertropical arcs were measured along with their red line brightness, with moderate success. Although the model showed arc brightness in places not observed by WINDII and

predicted brightnesses and a wind field that showed some quantitative disagreement with those observed, the simulation gave qualitative agreement with arc location and the dependence of brightness on meridional wind. The authors note that the TIEGCM for 27 October required equinox conditions for best simulation, which agrees with our calling September a summer month with regard to arc behavior. All of the comparisons were for specific pre-midnight local times with contours on grids of latitude vs. longitude rather than latitude vs. local time as used here, but we can expect that the TIEGCM simulation of our Asmara observations would also be qualitatively a good approximation. TIEGCM's success in simulating the pre-reversal enhancement, as reported by Fesen et al. (2000), suggests that our pre-midnight brightness enhancement caused by the enhanced fountain effect that results from this may also be possible, but these have not been attempted as far as we know. The midnight temperature maximum was simulated by Fesen (1996) who found it necessary to impose enhanced (2,2) and (2,3) tidal modes from the lower atmosphere, in addition to the ion-momentum coupling and the in situ EUV heating semidiurnal sources to produce a small temperature maximum at 03:00 LT on the equator at equinox. Such a fixed MPB would explain the persistence of our 02:00 LT brightness maximum, but we prefer the lateral V structure for its consistency with observations by others as well as our own. Detailed criticism of the TIEGCM simulation results is given by Colerico and Mendillo (2002), who recommend the use of higher order tidal modes. So far, the TIEGCM has only been used to simulate the MTM at equinox during a period of solar minimum. Goembel and Herrero (1995) have shown that the strength of the MPB depends upon the EUV flux, implying that our data, from a period of solar maximum, would be subject to stronger bulge effects than those thus far simulated by TIEGCM. In any case, the TIEGCM results do not yet appear directly applicable to our findings here.

As already discussed, our data agree best with the empirically determined lateral V structure of Herrero and Spencer (1982), although our interpretation demands symmetry across the geographic equator. Herrero et al. (1983) demonstrate the tidal interactions between semidiurnal modes of the in situ EUV heating and the ion-momentum coupling source that can produce seasonal variations, but their equations, including the two processes, have not been developed into a form that allows comparison with our data. When such a numerical model is developed, we would encourage that it be tested with data from a wide variety of ground-based longitudes.

5 Conclusion

All-sky imager data on the brightness of the 630 nm O(^{1}D) nightglow have been processed to show monthly averaged contours of uncalibrated brightness on a latitude vs. local time grid. Such contour plots are presented, one for each month from September 2001 to May 2002, during which the solar EUV, as characterized by the F10.7 index, was at the maximum of the solar cycle. The images were taken from Asmara, Eritrea just 7° north of the magnetic dip equator in eastern Africa. The monthly plots show the intertropical arc fully developed to the north of the station during the winter months. Its characteristics include a pre-midnight brightening, a brightness decrease at midnight, a strong and persistent post-midnight brightness maximum, and termination shortly before dawn. This description is consistent with early observations in this longitude sector, but much detail is added here. Although our summer data are limited, they indicate that in summer the pre-midnight arc disappears, but the post midnight brightening persists, varying in amplitude but fixed in location in all seasons. The winter pre-midnight brightening is attributed to an enhanced fountain effect related to the equatorial pre-reversal electric field enhancement. An interpretation of all the other brightenings and wanings in terms of meridional winds driving ions down or up the magnetic field lines has been offered. These meridional winds include those that blow from the summer into the cooler winter hemisphere and those driven by the MPB. An MPB structure that is centered on the geographic equator and extends to higher latitudes with increasing local time in both hemispheres, giving it a lateral V shape allows for an explanation of the unvarying location of the post-midnight brightness maximum in all months. Such a structure also accounts for the weak emission at midnight and the extinction of the intertropical arc before dawn. The primary mechanism for the bulge is a combination of semidiurnal thermospheric tides driven by ion momentum coupling and seasonally variable in situ solar EUV heating. The explicit shape of the bulge has not yet been predicted from first principles, assuming these as primary drivers. It is important to recognize that our data refer to the maximum of the solar activity cycle when the EUV heating tide will have its maximum amplitude. Further observations could determine to what extent the pattern described here applies during solar minimum.

Acknowledgements. The authors gratefully acknowledge material support in the form of YASAC from G. G. Shepherd. We are also grateful for numerous significant contributions from a patiently diligent and knowledgeable referee.

Topical Editor U.-P. Hoppe thanks C. Fesen and another referee for their help in evaluating this paper.

References

Abreu, V. J., Schmitt, G. A., Hays, P. B., and Dachev, T. P.: Volume emission rate profiles of the 6300-A tropical nightglow obtained from the AE-E satellite: latitudinal and seasonal variations, J. Geophys. Res., 87, 6346–6352, 1982.

Anderson, D. N.: A theoretical study of the ionospheric F region equatorial anomaly – II. Results in the American and Asian sectors, Planet. Space Sci., 21, 421–442, 1973.

Arduini, C., Laneve, G., and Herrero, F. A.: Local time and altitude variation of equatorial midnight density maximum: San Marco drag balance measurements, Geophys. Res. Lett. 24, 377–380, 1997.

Barbier, D. and Glaume, J.: La couche ionospherique nocturne F dans la zone intertropicale et ses relations avec l'emission de la raie 6300 A du ciel nocturne, Planet. Space Sci., 9, 133–148, 1962.

Barbier, D., Weill, G., and Glaume, J.: L'emission de la raie rouge du ciel nocturne en Afrique, Ann. Geophys. 17, 305–318, 1961.

Batista, I. S., Sastri, J. H., de Medeiros, R. T., and Abdu, M. A.: Nighttime thermospheric meridional winds at Cachoeira Paulista (23 S, 45 W): evidence for effects of the equatorial midnight pressure bulge, J. Geophys. Res., 102, 20 059–20 062, 1997.

Battaner, E. and Pardo, G.: On the motion of the tropical red arc north boundary, Ann. Geophys., 28, 755–756, 1972.

Behnke, R. A. and Harper, R. M.: Vector measurements of F region ion transport at Arecibo, J. Geophys. Res., 78, 8222–8234, 1973.

Chandra, S., Reed, E. I., Troy, B. E., and Blamont, J. E.: Equatorial airglow and the ionospheric geomagnetic anomaly, J. Geophys. Res., 78, 4630–4640, 1973.

Colerico, M. J. and Mendillo, M.: The current state of investigations regarding the thermospheric midnight temperature maximum (MTM), J. Atmos. S.-P., 64, 1361–1369, 2002.

Colerico, M. J., Mendillo, M., Nottingham, D., Baumgardner, J., Meriwether, J., Mirick, J., Reinisch, B. M., Scali, J. L., Fesen, C. G., and Biondi, M. A.: Coordinated measurements of F region dynamics related to the thermospheric midnight temperature maximum, J. Geophys. Res., 101, 26 783–26 793, 1996.

Criswick, J. R.: An all-sky imager for observing airglow activity in the upper atmosphere, M.Sc. Thesis, York University, Toronto, 1996.

Fesen, C. G.: Simulations of the low-latitude midnight temperature maximum, J. Geophys. Res., 101, 26 863–26 874, 1996.

Fesen, C. G., Crowley, G., Roble, R. G., Richmond, A. D., and Fejer, B. G.: Simulation of the pre-reversal enhancement in the low latitude vertical ion drifts, Geophys. Res. Lett., 27, 1851–1854, 2000.

Goembel, L. and Herrero, F. A.: Anomalous meridional thermospheric neutral winds in the AE-E NATE data: Effects of the equatorial nighttime pressure bulge, Geophys. Res. Lett., 22, 271–274, 1995.

Greenspan, J. A.: Synoptic description of the 6300A nightglow near 78° west longitude, J. Atmos. Terr. Phys., 28, 739–745, 1966.

Hanson, W. B. and Moffett, R. J.: Ionization transport effects in the equatorial F region, J. Geophys. Res., 71, 5559–5572, 1966.

Hari, S. S. and Krishna Murthy, B. V.: Seasonal variations of equatorial night-time thermospheric meridional winds, J. Atmos. S-P, 57, 1241–1246, 1995.

Harper, R. M.: Nighttime meridional neutral winds near 350 km at low to mid-latitudes, J. Atmos. Terr. Phys., 35, 2023–2034, 1973.

Hedin, A. E., Spencer, N. W., and Mayr, H. G.: The semidiurnal and terdiurnal tides in the equatorial thermosphere from AE-E measurements, J. Geophys. Res., 85, 1787–1791, 1980.

Herrero, F. A. and Mayr, H. G.: Tidal decomposition of zonal neutral and ion flows in the Earth's upper equatorial thermosphere, Geophys. Res. Lett., 13, 359–362, 1986.

Herrero, F. A. and Meriwether Jr., J. W.: 6300-A airglow meridional intensity gradients, J. Geophys. Res., 85, 4191–4204, 1980.

Herrero, F. A. and Spencer, N. W.: On the horizontal distribution of the equatorial thermospheric midnight temperature maximum and its seasonal variation, Geophys. Res. Lett., 9, 1179–1182, 1982.

Herrero, F. A., Mayr, H. G., and Spencer, N. W.: Latitudinal (seasonal) variations in the thermospheric midnight temperature maximum: A tidal analysis, J. Geophys. Res., 88, 7225–7235, 1983.

Herrero, F. A., Spencer, N. W., and Mayr, H. G.: Thermosphere and F-region plasma dynamics in the equatorial region, Adv. Space Res., 13, (1)201–(1)220, 1993.

Mayr, H. G., Harris, I., Spencer, N. W., Hedin, A. E., Wharton, L. E., Porter, H. S., Walker, J. C. G., and Carlson Jr., H. C.: Tides and the midnight temperature anomaly in the thermosphere, Geophys. Res. Lett., 6, 447–450, 1979.

Nelson, G. J. and Cogger, L. L.: Dynamical behaviour of the nighttime ionosphere at Arecibo, J. Atmos. Terr. Phys., 33, 1711–1726, 1971.

Ranganath Rao, H. N. and Sastri, J. H.: Characteristics of the equatorial midnight temperature maximum in the Indian sector, Ann. Geophys., 12, 276–278, 1994.

Sastri, J. H., Ranganath Rao, H. N., Somayajulu, V. V., and Chandra, H.: Thermospheric meridional neutral winds associated with equatorial midnight temperature maximum (MTM), Geophys. Res. Lett., 21, 825–828, 1994.

Skinner, N. J., Carman, E. H., and Heeran, M. P.: Movements of airglow structures within the intertropical arc observed from southern Kenya, J. Atmos. Terr. Phys., 39, 1395–1398, 1977.

Sobral, J. H. A., Carlson, H. C., Farley, D. T., and Swartz, W. E.: Nighttime dynamics of the F region near Arecibo as mapped by airglow features, J. Geophys. Res., 83, 2561–2566, 1978.

Spencer, N. W., Carignan, G. R., Mayr, H. G., Niemann, H. B., Theis, R. F., and Wharton, L. E.: The midnight temperature maximum in the earth's thermosphere observed at low latitudes, Geophys. Res. Lett., 6, 444–446, 1979.

Thuillier, G., King, J. W., and Slater, A. J.: An explanation of the longitudinal variation of the $O(^1D)$ 630 nm tropical nightglow intensity, J. Atmos. Terr. Phys., 38, 155–158, 1976.

Thuillier, G., Wiens, R. H., Shepherd, G. G., and Roble, R. G.: Photochemistry and dynamics in thermospheric intertropical arcs measured by the WIND Imaging Interferometer on board UARS: a comparison with TIE-GCM simulations, J. Atmos. S.-P., 64, 405–415, 2002.

Weill, G., Fehrenbach, M., Morguleff, N., and Christophe-Glaume, J.: The forbidden lines of OI and NI in the night airglow at the magnetic equator, Ann. Geophys., 24, 109–114, 1968.

Whalen, J. A.: Appleton anomaly increase following sunset: its observed relation to equatorial F layer $E \times B$ drift velocity, J. Geophys. Res., 103, 9497–9503, 1998.